This is the accepted manuscript made available via CHORUS. The article has been published as:

Gate-tunable quantum anomalous Hall effects in math xmlns="http://www.w3.org/1998/Math/MathML">msub>mrow>mi>MnBi/mi>/mrow>mn>2/mn>/msub>msub>mrow>mi>Te/mi>/mrow>mn>4/mn>/msub>/math> thin films

Chao Lei and A. H. MacDonald

Phys. Rev. Materials **5**, L051201 — Published 27 May 2021

DOI: 10.1103/PhysRevMaterials.5.L051201

Gate-Tunable Quantum Anomalous Hall Effects in $MnBi_2Te_4$ Thin Films

Chao Lei and A. H. MacDonald[1]

[1] *Department of Physics, The University of Texas at Austin, Austin, Texas 78712, USA*

(Dated: May 17, 2021)

The quantum anomalous Hall (QAH) effect has recently been realized in thin films of intrinsic magnetic topological insulators (IMTIs) like $MnBi_2Te_4$. Here we point out that that the QAH gaps of these IMTIs can be optimized, and that both axion insulator/semimetal and Chern insulator/semimetal transitions can be driven by electrical gate fields on the ~ 10 meV/nm scale. This effect is described by combining a simplified coupled-Dirac-cone model of multilayer thin films with Schrödinger-Poisson self-consistent-field equations.

Introduction— Following its initial experimental realization in magnetically-doped topological insulators (MTI)[1], the quantum anomalous Hall (QAH) effect[2] has been widely studied[3–7]. The QAH effect is of interest because of its potential applications in quantum metrology[8–10] and spintronics[11, 12], and because of its potential role as a platform for chiral topological superconductivity[13, 14], Majorana edge modes[15], and Majorana zero modes[16]. Because of strong disorder, thought to be due mainly to random magnetic dopants, the QAH effect appears only at extremely low temperatures in MTIs. Overcoming this disorder effect has been recognized as key to realizing the higher temperature QAH effects that would bring more applications within reach.

Topological materials with spatially ordered magnetic moments can be realized by forming heterojunctions between ferromagnetic insulators and topological insulators[4, 17–20] or by growing intrinsic $MnBi_2X_4$ or $MnSb_2X_4$ magnetic topological insualtors (IMTIs) and related superlattices [21–55], where X=(Se,Te). To date the anomalous Hall resistances measured[4, 17–20] in the heterojunction systems are still far from their ideal quantized values, mainly due to weak exchange coupling between the surface states of the topological insulator and moments in the ferromagnetic insulator. On the other hand, reasonably accurately quantized Hall resistances have been measured[37] in five-septuple layer thin films of $MnBi_2Te_4$ (MBT) in the absence of magnetic field (but not all [56]) at a temperature exceeding 1K and, in the presence of magnetic field $\sim$ 5T, at other film thicknesses[35, 37, 44] and higher temperatures.

Although the QAH temperature is larger in the IMTI case than in the magnetic-dopant case, the anomalous Hall resistances R_{xy} can deviate by as much as a factor of 3% from exact quantization and the longitudinal resistances R_{xx} are still $\sim 0.01 - 0.02h/e^2$. This compares with Hall resistivity deviations smaller than 1 ppm [9, 10] at the lowest temperatures in the magnetic-dopant case. In this paper, we theoretically explore the possibility of optimizing the QAH in MBT by applying electrical gate voltages to increase the QAH gap, and also address gate-tuned transitions between insulating and semimetallic states, and in the case of ferromagnetic spin configurations between insulating states with different Chern numbers.

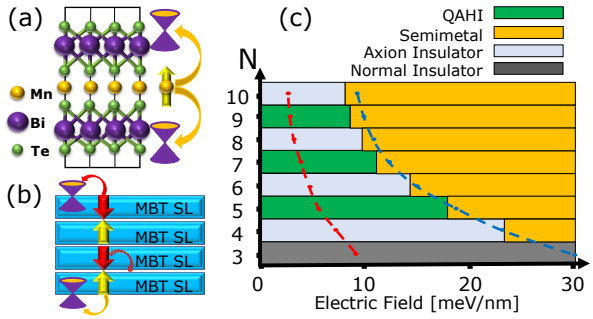


FIG. 1. (a) Crystal structure of one septuple layer of MBT, which consists of seven layers with one magnetic Mn ion in the center and two Te-Bi-Te trilayers outside; Two Dirac cones lie at the surface. (b) Coupling between surface layer Dirac cones and the local moments present in antiferromagnetic MBT thin films. The Dirac-cone masses are produced by exchange coupling to the Mn local moments (red and yellow arrows), and are opposite (identical) in sign on opposite surfaces for even (odd) layer-number thin films. (c) Phase diagram of antiferromagnetic thin films *vs.* electric field and the number of septuple layers N. Different colors represent different phases. The red and blue dashed lines respectively plot the electric fields E at which $eEt_N = E_{gs}$ and $eEt_N/\epsilon_{zz} = E_{gs}$ (See main text.)

Our analysis is based on the simplified coupled Dirac-cone model[21] illustrated schematically in Fig. 1 (a) and (b)) that captures most topological and electronic properties, and on a self-consistent-field Schödinger-Possion approximation for the interacting carriers. We show that gates can maximize the QAH gap either by compensating for unintentional electric fields, or in the case of high-Chern-number ferromagnetic (FM) insulators, by tuning the gate field to an optimal non-zero value.

Gate-Field Phase Diagram— The low-energy properties of MBT thin films are accurately modeled [21, 57] by a simple Hamiltonian that includes only Dirac cone surface states on the top and bottom surface of each septuple layer (as illustrated in Fig. 1 (a)), and hopping

between Dirac cones:

$$H = \sum_{\mathbf{k}_\perp, ij} \Big[\Big((-)^i \hbar v_{_D} (\hat{z} \times \sigma) \cdot \mathbf{k}_\perp + m_i \sigma_z + V_i \Big) \delta_{ij} + \Delta_{ij}(1-\delta_{ij}) \Big] c^\dagger_{\mathbf{k}_\perp i} c_{\mathbf{k}_\perp j} \ . \quad (1)$$

Here the Dirac cone labels i and j are respectively odd and even on the top and bottom surface of each septuple layer, $\hbar$ is the reduced Planck's constant, $v_{_D}$ is the Dirac-cone velocity and V_i is the self-consistent Hartree potential on surface i. $m_i = \sum_\alpha J_{i\alpha} M_\alpha$ where α is a layer label and $M_\alpha = \pm 1$ specifies the sense of magnetization on layer α. In this paper we set the parameters as Δ_S=84 meV, Δ_D = -127 meV, J_S = 36 meV and J_D = 29 meV, (S/D denotes the ones from the same/different layer) based on the fit to $MnBi_2Te_4$ *ab initio* electronic structure calculations discussed in detail in Ref. 21.

The Dirac-cone Hartree potentials V_i in Eq. 1 are calculated from a discrete Poisson equation in which positions z_i are assigned to Dirac-cone states ordered sequentially from top to bottom. The position assignments are based on microscopic charge-density-weighted average positions discussed in the Supplementary Material[58]. The discrete Poisson equation reads

$$\begin{aligned} \tilde{\epsilon}\mathcal{E}_i &= \tilde{\epsilon}\mathcal{E}_t + \sum_{j=1}^{i} \delta\rho_i = \tilde{\epsilon}\mathcal{E}_{i-1} + \delta\rho_i, \\ V_i &= \sum_{j=2}^{i} \mathcal{E}_i (z_i - z_{i-1}) = V_{i-1} + \mathcal{E}_i (z_i - z_{i-1}) \ . \end{aligned} \quad (2)$$

Here $\mathcal{E}_t = \mathcal{E}_0$ is the electric field controlled by the top gate above the top surface of the thin film, $\mathcal{E}_i$ is the electric field between surface i and $i+1$, $\tilde{\epsilon}$ is intended to account for gate field screening by degrees of freedom not included in our model, and V_i and $\delta\rho_i$ are the Hartree-potential and net surface charge density at surface i. (We choose $V_1 = 0$.) The bulk perpendicular dielectric constant ϵ_{zz} of MBT has not been measured, to our knowledge, but should be close to $\epsilon_{zz} \sim 3$ measured in Bi_2Te_3 [59]. We obtain the bulk dielectric constant of the Dirac cone model from the imaginary part of the conductivity using the general relationship

$$\epsilon_{zz} = 1 + 4\pi i \lim_{\omega \to 0} \frac{\partial \sigma_{zz}(\omega)}{\partial \omega}, \quad (3)$$

where $\sigma_{zz}(\omega)$ is the optical conductivity [58]. We find by explicit calculation that the Dirac cone model's bulk dielectric constant $\epsilon_{zz} \sim 3.5$ for the model parameters used here. We have therefore concluded that most of the perpendicular screening in MBT is captured by the Dirac cone model and set $\tilde{\epsilon} = 1$ in all the explicit calculations we describe. The surface charge densities used in the Poisson equation are calculated self-consistently from the electronic structure model using

$$\rho_i = -e \int \frac{d\mathbf{k}}{(2\pi)^2} \sum_{n=1}^{4N} \sum_{s=\uparrow,\downarrow} |\Psi^\sigma_{n\mathbf{k}}(z_i)|^2 f(E_{n\mathbf{k}} - \mu), \quad (4)$$

where e is electron charge, n is a quasi-2D band label, $f(E_{n\mathbf{k}} - \mu)$ is the Fermi-Dirac distribution function, and μ is the chemical potential. The net surface charge density $\delta\rho_i$, which appears in the Poisson equation, is defined as the difference between ρ_i calculated from Eq. 4 and the charge density ρ_i^0 calculated from the same equation with the Fermi level in the gap and no gate field, i.e. $\delta\rho_i \equiv \rho_i - \rho_i^0$. This prescription is motivated by the linearity of the Poisson equation, and by the fact that the bare bands have been fit to the electronic structure of neutral ungated thin films.

For a thin film with N septuple layers, the model has $2N$ Dirac cones located at the surfaces of each septuple layer and $4N$ bands, $2N$ of which are occupied at neutrality and temperature $T = 0$ – the limit considered in this paper. The electric field below the bottom layer of the thin film $\mathcal{E}_b = \mathcal{E}_t$ at neutrality. The antiferromagnetic (AF) thin film phase diagrams obtained from these self-consistent Hartree calculations are summarized in Fig. 1 (c), from which it follows that the thin films become semimetals when the electric field exceeds a critical value. This critical field decreases when the thickness of thin film increases and asymptotically approaches $E_{gs}\epsilon_{zz}/t_N$, where $E_{gs} \sim 37$ meV is the surface state energy gap [21] and t_N is the thickness of an N septuple layer film. To test the reliability of the simplified electronic structure model in accounting for gate-field response, we performed corresponding DFT calculations of the electron structure of MBT thin film with 2-6 septuple layers. The critical fields using the two approaches are in qualitative agreement[58], although there are some quantitative differences between Scrödinger-Poisson equation and DFT solutions. We attribute these differences mainly to inaccuracies in the estimates of thin film gaps at zero-electric field. The critical electric fields estimated from DFT are in principle more accurate because they explicitly include screening by high energy electronic degrees of freedom, the exchange-correlation corrections, and the differences in the exchange interactions with local moments in layers closer to the surface. We do not consider these quantitative discrepancies to be of great signficance, partly because both approaches are approximate - LDA approximations for exchange and correlations are suspect when bands have a lot of topological character, and in van der Waals materials.

At small electric fields, the thin films exhibit an even-odd effect, namely that thin films with an even number of septuple layers are axion insulators with strong magneto-electric response properties [25, 60], whereas those with an odd layer-number ($N > 3$) are QAH insulators [21]. We regard $N = 3$ films as normal two-dimensional insulators since they do not have the strong magneto-electric response present in even-N thin films regarded as axion insulators. The even-odd effect is illustrated schematically in Fig. 1 (b), we can see that the Dirac cones at the top and bottom surfaces have opposite masses for even layer-number thin films, but have identical masses for odd layer-number films [58].

Gate-control of the QAH effect — In antiferromagnetic MBT thin films QAH resistances are expected when the number of septuples N is odd. Under these circumstances the film has residual magnetism due to uncompensated moments, DFT calculations[34] predict that the QAH effect occurs for three or more layers, and a robust QAH effect has been measured in high-quality 5-layer MBT thin film[37].

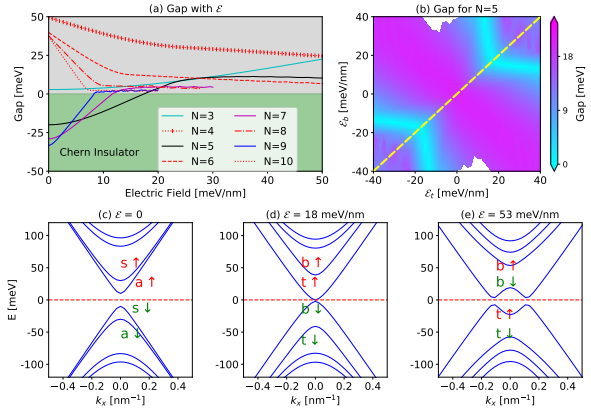


FIG. 2. (a) Gap *vs.* gate electric field for N-septuple layer charge-neutral antiferromagnetic thin films. A negative sign is assigned to the gaps when the Chern number is non-zero, to facilitate identification of topologically non-trivial states. The green (grey) shaded regions contain Chern (trivial/semimetal) insulator phase. (b) Gap *vs.* gate electric fields for five-septuple-layer thin films. Neutrality occurs along the yellow dashed line. There is no data in the white region due to the mapping from a numerical $\mathcal{E}_t - \mu$ grid to the $\mathcal{E}_t - \mathcal{E}_b$ grid. (c)-(d) Self-consistent bandstructures of neutral five-septuple-layer thin films. In (c) the bands are labeled as layer symmetric (s) or anti-symmetric(a) and by majority spin (↑ or ↓). In (c) and (d) bands are labelled by majority surface (t for top or b for bottom) and spin.

In Fig.2 (a) we plot the gaps of several MBT thin films *vs.* gate electric field. For even N all insulators have zero Chern number, and gaps decrease with the gate fields. With the parameters we have chosen, N=3 thin film is trivial, but an increase of the magnetic exchange coupling parameters by as little as several meV would drive the system from a trivial insulator state to a Chern insulator state. If the ideal ungated three-septuple layer antiferromagnetic MBT thin film is indeed a trivial insulator, our calculations show that a gate field would not be able to drive the system into a Chern insulator state since the condition to be a Chern insulator is $m > \sqrt{\Delta^2 + V^2}$ [58] in the presence of electric field. Here m,Δ,V are the parameters of the mass, hybridization of top and bottom surface states, and Hartree potential induce by the electric field in the toy model illustrated in the supplemental material. On the other hand, a small electric field due to asymmetric unintended doping would close the gap of the Chern insulator state [58, 61], even if it were stable in the ideal case. In contrast odd N films with $N \geq 5$ all have robust QAH effects in the absence of a gate field as shown in Fig. 2 (a) where we see that gate fields always act to reduce thin film gaps. The ideal QAHE gap cannot be enhanced by gate fields, but dual gating will still be valuable in practice since real samples normally have unintended electric fields for which the gate fields can compensate. This behavior can be understood qualitatively as a consequence of an energetic shift of the magnetically gapped states on one surface relative to those on the other surface so that the conduction band states of the low-potential energy surface fall below the top of the valence band on the high-potential energy surface. The gaps tend to survive to larger gate electric fields for even N than for odd N because the approaching valence and conduction band extrema states have the same dominant spin in the former case, strengthening level repulsion effects. In the limit of thick films the critical electric field E required to close the gap approaches the value $E_{gs}\epsilon_{zz}/et_N$ where $E_{gs} \sim 37$ meV is the energy gap of isolated surface states.

The energy gap in the quasi-2D band structure of the $N = 5$ thin film is plotted *vs.* top and bottom gate fields in Fig. 2 (b), where the yellow dashed line marks the neutrality line. We see here that as the carrier densities of the films increase, the overall gap is controlled more and more by the independent screening of external electric fields by carriers near either surface. When carriers are present, the screened electric field drops toward near the middle of thick films and larger electric fields are generally required to close the gap. Of course, when the Fermi level does not lie in the gap and away from the neutrality line, the resulting states are magnetically ordered two-dimensional Fermi liquids with large momentum-space Berry curvatures [62], not Chern insulators. Because these itinerant electron ferromagnets are strongly gate-tunable, they are potentially interesting for spintronics.

The band structure evolution with the gate field for $N = 5$ neutral antiferromagnets is illustrated in Fig. 2 (c)-(e). In these plots we have labeled the subbands based on the projection of their wavefunctions to individual spins, and to Dirac cones associated with particular septuple layers. For $N = 5$ antiferromagnets, the Hamiltonian in the absence of a gate field (Fig. 2 (c)) possesses a $z \to -z$ mirror symmetry which leads to band eigenstates that are either symmetric (s) or antisymmetric (a) under this symmetry operation. At finite gate fields, the four subbands around the Fermi level reside mainly on the top or bottom surfaces (t for top and b for bottom) of the thin film and they are strongly spin-polarized (↑ or ↓) [58]. Either $t\uparrow$ and $b\downarrow$ or $t\downarrow$ and $b\uparrow$ subbands lie close to the Fermi level depending on the direction of the electric field and the spin-configuration. Fig. 2 (d) shows the bands near the critical value at which band touching first occurs, near 18 meV/nm for $\epsilon_{zz} \sim 3.5$. At larger fields (Fig. 2 (e)), the $b\downarrow$ and $t\uparrow$ subbands are inverted. The inversion changes the polarizations of the subband just below Fermi level, and drives the thin film from a state with Chern number $C = 1$ to semimetal state with $C = 0$.

In the semimetal state beyond the critical electric field, a small gap reopens in our simplified electron-structure model due to weak-coupling between the top and bottom surfaces. These small gaps are not expected to survive in more realistic models because of their anisotropic band dispersion. When the critical electric field is exceeded, conduction band states on one surface of the film overlap in energy with valence band states localized mainly on the opposite surface. Avoided crossing between these two sets of bands is responsible for the small gaps that open in our model calculations. The trigonal anisotropy of realistic bands means that the avoided crossings will occur at different energies for different directions, disallowing overall gaps.

High-Chern-number QAH Systems— Because their antiferromagnetic interlayer exchange interactions are exceptionally weak, The Mn local moment spins in MBT are aligned by external magnetic fields larger than ~ 5 Tesla [35, 37, 44]. Since bulk ferromagnetic MBT is a Weyl semimetal, in the thick film limit, the Chern number per layer of a ferromagnetic MBT film approaches the dimensionless Hall conductivity per layer of the bulk semimetal (~ 0.2), with finite-size energy gaps that tend to get smaller as the films get thicker. The Chern number of ferromagnetic MBT thin films with $N > 8$ are larger than 1 [21, 44] in the absence of a gate field. In Fig. 3 (a) we show the gaps *vs.* gate electric fields for FM thin films with N from 7 to 10, crossing the thickness at which the Chern number jumps from 1 to 2 at zero electric field. Overall the gaps tend to decrease with the gate field as in the antiferromagnetic case. An exception occurs for the $N = 9$ and $N = 10$ films, for which the gaps initially increase as the system moves further from the $C = 2$ to $C = 1$ boundary with the gate field. In Fig. 3 (b), where we assign a positive sign to the gap of odd-Chern-number(C=1) states and a negative sign for even-Chern-number(C=0 or 2) states, we illustrate the thickness dependence for a series of gate fields. Gate electric fields can induce transitions between insulators with different Chern numbers as illustrated in Fig. 3 (c).

The green and magenta curves for $N = 9$ and $N = 10$ in Fig. 3 (a) show that the maximum QAH gaps are reached at around 10-15 meV/nm. At around 25 meV/nm, a topological phase transition occurs at which the Chern numbers change from 2 to 1, and further change to 0 as the electric fields increase (shown as in Fig. 3 (c)). These transitions are illustrated further in Fig. 3 (d) and (e), where we show the bandstructures of FM thin films with $N = 9$ in Fig. 3 (d) and (e), with zero electric field (red dashed curve in (d)), with electric field $\mathcal{E} = 15$ meV/nm (blue curve in (d)), and with electric field $\mathcal{E} = 25$ meV/nm (in (e)). Unlike the bandstructures of the AF thin film with $N = 5$ in Fig.2, the bands closest to the Fermi level are not located primarily in the $t\uparrow$ and $b\downarrow$ septuple layers and are instead spread across the thin film. As the electric field increases, the $t\uparrow$ subband is pushed down and the $b\downarrow$ subbands are pulled up. Before these two subbands touch up at $\mathcal{E} \sim 25$ meV/nm

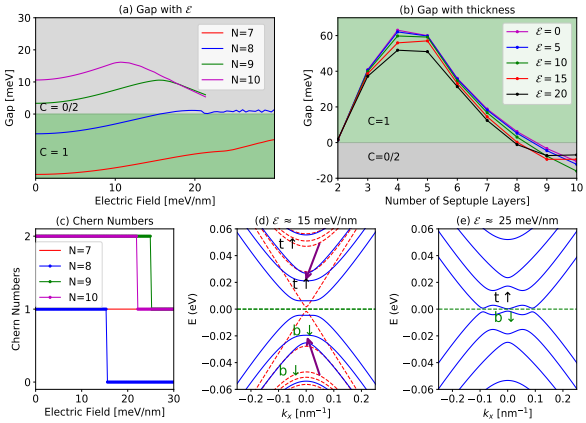


FIG. 3. (a) Gaps *vs.* gate electric fields for ferromagnetic thin films from 7 to 10 septuple layers. For the $N = 7$ thin film no gap closing happens occurs below 30 meV/nm, whereas for the $N = 8$ thin film, the QAH gap closes at $\mathcal{E} \sim 17$ meV/nm, For N =9/10 thin films, the QAH gap closes at $\mathcal{E} \sim 25$ meV/nm; (b) QAH gaps *vs.* thickness for several electric fields from $\mathcal{E} = 0$ to $\mathcal{E} = 20$ meV/nm; (c) Chern numbers *vs.* electric field for several film thicknesses from $N = 7$ to $N = 10$; (d) and (e) are bandstructure of $N = 9$ ferromagnetic thin film in different electric fields.

(shown in Fig. 3(e)), hybridization between the electron and hole subbands spread across the entire thin film [58] increases and thus increase the QAH gap. When the $t\uparrow$ and $b\downarrow$ subbands touch at $\mathcal{E} \sim 25$ meV/nm, a topological phase transition occurs at which the Chern number changes from 2 to 1. Similar band inversions occur for the other two subbands which are not shown in the figure, and eventually change the Chern number from 1 to 0.

Discussion— In summary, we have studied gate tuning effects in MBT thin films using self-consistent Schrödinger-Poisson equations, demonstrating that gates can optimize the QAH gap either by compensating for unintentional electric fields, or in the case of high-Chern-number ferromagnetic (FM) insulators, by tuning the gate field to an optimal non-zero value. Our theory provides an explanation for the absence of the QAH effect in AF thin film with three septuple layers, and sheds light on strategies to optimize the QAH effect in both antiferromagnetic and ferromagnetic MBT thin films using gates. The gate electric fields that induce large changes are on the scale of 10 meV/nm, which is easily realized experimentally. Although many of the film geometries we have studied are also addressable with microscopic DFT, it requires considerably more computational resources than the couple Dirac cone model as the film thicknesses increases [58].

In this paper, we have focused on neutral MBT thin films in this paper, however, gate-tuning is phenomenologically richer in the case of electrostatic doping, where the ground states are expected to be extremely tunable magnetically ordered two-dimensional metals. The

Hall effect will remain quantized in doped samples, provided that the added charges are localized. Since magnetization textures are charged in Chern insulators, we anticipate the possibility of engineering Skyrmion lattice ground states[63–66] at finite doping. Separately, strong gate fields can be used to engineer strong spin-orbit coupling[67, 68], in Fermi liquid states and to control the interplay between the itinerant electron and Mn local moment contributions to the magnetization.

I. ACKNOWLEDGEMENTS

This work was sponsored by the Army Research Office under Grant Number W911NF-16-1-0472. We acknowledge helpful discussions with Anton Burkov, Gaurav Chaudhary, Paul Haney, Olle Heinonen, Rob McQueeney, Suyang Xu and Fei Xue. The authors acknowledge the Texas Advanced Computing Center (TACC) at The University of Texas at Austin for providing HPC resources that have contributed to the research results reported in this paper.

[1] C.-Z. Chang, J. Zhang, X. Feng, J. Shen, Z. Zhang, M. Guo, K. Li, Y. Ou, P. Wei, L.-L. Wang, Z.-Q. Ji, Y. Feng, S. Ji, X. Chen, J. Jia, X. Dai, Z. Fang, S.-C. Zhang, K. He, Y. Wang, L. Lu, X.-C. Ma, and Q.-K. Xue, Science **340**, 167 (2013).
[2] F. D. M. Haldane, Phys. Rev. Lett. **61**, 2015 (1988).
[3] C.-X. Liu, S.-C. Zhang, and X.-L. Qi, Annual Review of Condensed Matter Physics **7**, 301 (2016).
[4] Y. Tokura, K. Yasuda, and A. Tsukazaki, Nature Reviews Physics **1**, 126 (2019).
[5] A. J. Bestwick, E. J. Fox, X. Kou, L. Pan, K. L. Wang, and D. Goldhaber-Gordon, Phys. Rev. Lett. **114**, 187201 (2015).
[6] X. Kou, S.-T. Guo, Y. Fan, L. Pan, M. Lang, Y. Jiang, Q. Shao, T. Nie, K. Murata, J. Tang, Y. Wang, L. He, T.-K. Lee, W.-L. Lee, and K. L. Wang, Phys. Rev. Lett. **113**, 137201 (2014).
[7] X. Kou, L. Pan, J. Wang, Y. Fan, E. S. Choi, W.-L. Lee, T. Nie, K. Murata, Q. Shao, S.-C. Zhang, *et al.*, Nature communications **6**, 1 (2015).
[8] Y. Okazaki, T. Oe, M. Kawamura, R. Yoshimi, S. Nakamura, S. Takada, M. Mogi, K. S. Takahashi, A. Tsukazaki, M. Kawasaki, Y. Tokura, and N.-H. Kaneko, Applied Physics Letters **116**, 143101 (2020).
[9] M. Götz, K. M. Fijalkowski, E. Pesel, M. Hartl, S. Schreyeck, M. Winnerlein, S. Grauer, H. Scherer, K. Brunner, C. Gould, F. J. Ahlers, and L. W. Molenkamp, Applied Physics Letters **112**, 072102 (2018).
[10] E. J. Fox, I. T. Rosen, Y. Yang, G. R. Jones, R. E. Elmquist, X. Kou, L. Pan, K. L. Wang, and D. Goldhaber-Gordon, Phys. Rev. B **98**, 075145 (2018).
[11] J. Wu, J. Liu, and X.-J. Liu, Phys. Rev. Lett. **113**, 136403 (2014).
[12] C.-Z. Chang, W. Zhao, D. Y. Kim, P. Wei, J. K. Jain, C. Liu, M. H. W. Chan, and J. S. Moodera, Phys. Rev. Lett. **115**, 057206 (2015).
[13] L. Fu and C. L. Kane, Phys. Rev. Lett. **100**, 096407 (2008).
[14] J. Wang, Q. Zhou, B. Lian, and S.-C. Zhang, Phys. Rev. B **92**, 064520 (2015).
[15] Q. L. He, L. Pan, A. L. Stern, E. C. Burks, X. Che, G. Yin, J. Wang, B. Lian, Q. Zhou, E. S. Choi, and et al., Science **357**, 294–299 (2017).
[16] Y. Zeng, C. Lei, G. Chaudhary, and A. H. MacDonald, Phys. Rev. B **97**, 081102 (2018).
[17] P. Wei, F. Katmis, B. A. Assaf, H. Steinberg, P. Jarillo-Herrero, D. Heiman, and J. S. Moodera, Phys. Rev. Lett. **110**, 186807 (2013).
[18] C. Lee, F. Katmis, P. Jarillo-Herrero, J. S. Moodera, and N. Gedik, Nature communications **7**, 1 (2016).
[19] F. Katmis, V. Lauter, F. S. Nogueira, B. A. Assaf, M. E. Jamer, P. Wei, B. Satpati, J. W. Freeland, I. Eremin, D. Heiman, *et al.*, Nature **533**, 513 (2016).
[20] M. Lang, M. Montazeri, M. C. Onbasli, X. Kou, Y. Fan, P. Upadhyaya, K. Yao, F. Liu, Y. Jiang, W. Jiang, *et al.*, Nano letters **14**, 3459 (2014).
[21] C. Lei, S. Chen, and A. H. MacDonald, Proceedings of the National Academy of Sciences **117**, 27224–27230 (2020).
[22] M. M. Otrokov, T. V. Menshchikova, M. G. Vergniory, I. P. Rusinov, A. Yu Vyazovskaya, Y. M. Koroteev, G. Bihlmayer, A. Ernst, P. M. Echenique, A. Arnau, and et al., 2D Materials **4**, 025082 (2017).
[23] S. Eremeev, M. Otrokov, and E. Chulkov, Journal of Alloys and Compounds **709**, 172–178 (2017).
[24] M. M. Otrokov, I. I. Klimovskikh, H. Bentmann, D. Estyunin, A. Zeugner, Z. S. Aliev, S. Gaß, A. U. B. Wolter, A. V. Koroleva, A. M. Shikin, and et al., Nature **576**, 416–422 (2019).
[25] D. Zhang, M. Shi, T. Zhu, D. Xing, H. Zhang, and J. Wang, Phys. Rev. Lett. **122**, 206401 (2019).
[26] J. Li, Y. Li, S. Du, Z. Wang, B.-L. Gu, S.-C. Zhang, K. He, W. Duan, and Y. Xu, Science Advances **5**, eaaw5685 (2019).
[27] S. Chowdhury, K. F. Garrity, and F. Tavazza, npj Computational Materials **5** (2019), 10.1038/s41524-019-0168-1.
[28] D. S. Lee, T.-H. Kim, C.-H. Park, C.-Y. Chung, Y. S. Lim, W.-S. Seo, and H.-H. Park, CrystEngComm **15**, 5532 (2013).
[29] E. D. L. Rienks, S. Wimmer, J. Sánchez-Barriga, O. Caha, P. S. Mandal, J. Růžička, A. Ney, H. Steiner, V. V. Volobuev, H. Groiss, and et al., Nature **576**, 423–428 (2019).
[30] A. Zeugner, F. Nietschke, A. U. B. Wolter, S. Gaß, R. C. Vidal, T. R. F. Peixoto, D. Pohl, C. Damm, A. Lubk, R. Hentrich, and et al., Chemistry of Materials **31**, 2795–2806 (2019).
[31] J.-Q. Yan, Q. Zhang, T. Heitmann, Z. Huang, K. Y. Chen, J.-G. Cheng, W. Wu, D. Vaknin, B. C. Sales, and R. J. McQueeney, Phys. Rev. Materials **3**, 064202 (2019).
[32] S. H. Lee, Y. Zhu, Y. Wang, L. Miao, T. Pillsbury, H. Yi, S. Kempinger, J. Hu, C. A. Heikes, P. Quarterman, W. Ratcliff, J. A. Borchers, H. Zhang, X. Ke, D. Graf,

N. Alem, C.-Z. Chang, N. Samarth, and Z. Mao, Phys. Rev. Research **1**, 012011 (2019).
[33] B. Li, J.-Q. Yan, D. M. Pajerowski, E. Gordon, A.-M. Nedić, Y. Sizyuk, L. Ke, P. P. Orth, D. Vaknin, and R. J. McQueeney, Phys. Rev. Lett. **124**, 167204 (2020).
[34] M. M. Otrokov, I. P. Rusinov, M. Blanco-Rey, M. Hoffmann, A. Y. Vyazovskaya, S. V. Eremeev, A. Ernst, P. M. Echenique, A. Arnau, and E. V. Chulkov, Phys. Rev. Lett. **122**, 107202 (2019).
[35] C. Liu, Y. Wang, H. Li, Y. Wu, Y. Li, J. Li, K. He, Y. Xu, J. Zhang, and Y. Wang, Nature Materials **19**, 522–527 (2020).
[36] K. Y. Chen, B. S. Wang, J.-Q. Yan, D. S. Parker, J.-S. Zhou, Y. Uwatoko, and J.-G. Cheng, Phys. Rev. Materials **3**, 094201 (2019).
[37] Y. Deng, Y. Yu, M. Z. Shi, Z. Guo, Z. Xu, J. Wang, X. H. Chen, and Y. Zhang, Science **367**, 895–900 (2020).
[38] H. Deng, Z. Chen, A. Wołoś, M. Konczykowski, K. Sobczak, J. Sitnicka, I. V. Fedorchenko, J. Borysiuk, T. Heider, Ł. Pluciński, and et al., Nature Physics (2020), 10.1038/s41567-020-0998-2.
[39] Y. Gong, J. Guo, J. Li, K. Zhu, M. Liao, X. Liu, Q. Zhang, L. Gu, L. Tang, X. Feng, and et al., Chinese Physics Letters **36**, 076801 (2019).
[40] S. Zhang, R. Wang, X. Wang, B. Wei, B. Chen, H. Wang, G. Shi, F. Wang, B. Jia, Y. Ouyang, and et al., Nano Letters **20**, 709–714 (2019).
[41] H. Li, S.-Y. Gao, S.-F. Duan, Y.-F. Xu, K.-J. Zhu, S.-J. Tian, J.-C. Gao, W.-H. Fan, Z.-C. Rao, J.-R. Huang, J.-J. Li, D.-Y. Yan, Z.-T. Liu, W.-L. Liu, Y.-B. Huang, Y.-L. Li, Y. Liu, G.-B. Zhang, P. Zhang, T. Kondo, S. Shin, H.-C. Lei, Y.-G. Shi, W.-T. Zhang, H.-M. Weng, T. Qian, and H. Ding, Phys. Rev. X **9**, 041039 (2019).
[42] Y.-J. Hao, P. Liu, Y. Feng, X.-M. Ma, E. F. Schwier, M. Arita, S. Kumar, C. Hu, R. Lu, M. Zeng, Y. Wang, Z. Hao, H.-Y. Sun, K. Zhang, J. Mei, N. Ni, L. Wu, K. Shimada, C. Chen, Q. Liu, and C. Liu, Phys. Rev. X **9**, 041038 (2019).
[43] Y. J. Chen, L. X. Xu, J. H. Li, Y. W. Li, H. Y. Wang, C. F. Zhang, H. Li, Y. Wu, A. J. Liang, C. Chen, S. W. Jung, C. Cacho, Y. H. Mao, S. Liu, M. X. Wang, Y. F. Guo, Y. Xu, Z. K. Liu, L. X. Yang, and Y. L. Chen, Phys. Rev. X **9**, 041040 (2019).
[44] J. Ge, Y. Liu, J. Li, H. Li, T. Luo, Y. Wu, Y. Xu, and J. Wang, National Science Review **7**, 1280–1287 (2020).
[45] C. Hu, K. N. Gordon, P. Liu, J. Liu, X. Zhou, P. Hao, D. Narayan, E. Emmanouilidou, H. Sun, Y. Liu, and et al., Nature Communications **11**, 1 (2020).
[46] L. Ding, C. Hu, F. Ye, E. Feng, N. Ni, and H. Cao, Phys. Rev. B **101**, 020412 (2020).
[47] P. Swatek, Y. Wu, L.-L. Wang, K. Lee, B. Schrunk, J. Yan, and A. Kaminski, Phys. Rev. B **101**, 161109 (2020).
[48] S. V. Eremeev, M. M. Otrokov, and E. V. Chulkov, Nano letters **18**, 6521 (2018).
[49] J. Wu, F. Liu, M. Sasase, K. Ienaga, Y. Obata, R. Yukawa, K. Horiba, H. Kumigashira, S. Okuma, T. Inoshita, and et al., Science Advances **5**, eaax9989 (2019).
[50] R. C. Vidal, A. Zeugner, J. I. Facio, R. Ray, M. H. Haghighi, A. U. B. Wolter, L. T. Corredor Bohorquez, F. Caglieris, S. Moser, T. Figgemeier, T. R. F. Peixoto, H. B. Vasili, M. Valvidares, S. Jung, C. Cacho, A. Alfonsov, K. Mehlawat, V. Kataev, C. Hess, M. Richter, B. Büchner, J. van den Brink, M. Ruck, F. Reinert, H. Bentmann, and A. Isaeva, Phys. Rev. X **9**, 041065 (2019).
[51] I. I. Klimovskikh, M. M. Otrokov, D. Estyunin, S. V. Eremeev, S. O. Filnov, A. Koroleva, E. Shevchenko, V. Voroshnin, A. G. Rybkin, I. P. Rusinov, *et al.*, npj Quantum Materials **5**, 1 (2020).
[52] H. Sun, B. Xia, Z. Chen, Y. Zhang, P. Liu, Q. Yao, H. Tang, Y. Zhao, H. Xu, and Q. Liu, Phys. Rev. Lett. **123**, 096401 (2019).
[53] M. Gu, J. Li, H. Sun, Y. Zhao, C. Liu, J. Liu, and Q. Liu, "Surface anomalous hall effect and its quantization in magnetic topological crystals," (2020), arXiv:2005.13943 [cond-mat.mes-hall].
[54] S. Wimmer, J. Sánchez-Barriga, P. Küppers, A. Ney, E. Schierle, F. Freyse, O. Caha, J. Michalicka, M. Liebmann, D. Primetzhofer, M. Hoffmann, A. Ernst, M. M. Otrokov, G. Bihlmayer, E. Weschke, B. Lake, E. V. Chulkov, M. Morgenstern, G. Bauer, G. Springholz, and O. Rader, "Ferromagnetic mnsb2te4: A topological insulator with magnetic gap closing at high curie temperatures of 45-50 k," (2020), arXiv:2011.07052 [cond-mat.mtrl-sci].
[55] I. Belopolski, S.-Y. Xu, N. Koirala, C. Liu, G. Bian, V. N. Strocov, G. Chang, M. Neupane, N. Alidoust, D. Sanchez, H. Zheng, M. Brahlek, V. Rogalev, T. Kim, N. C. Plumb, C. Chen, F. Bertran, P. Le Fèvre, A. Taleb-Ibrahimi, M.-C. Asensio, M. Shi, H. Lin, M. Hoesch, S. Oh, and M. Z. Hasan, Science Advances **3** (2017), 10.1126/sciadv.1501692.
[56] D. Ovchinnikov, X. Huang, Z. Lin, Z. Fei, J. Cai, T. Song, M. He, Q. Jiang, C. Wang, H. Li, and et al., Nano Letters **21**, 2544–2550 (2021).
[57] A. A. Burkov and L. Balents, Phys. Rev. Lett. **107**, 127205 (2011).
[58] See Supplemental Material for more information.
[59] J. Dheepa, R. Sathyamoorthy, A. Subbarayan, S. Velumani, P. Sebastian, and R. Perez, Solar energy materials and solar cells **88**, 187 (2005).
[60] T. Zhu, H. Wang, H. Zhang, and D. Xing, (2020), arXiv:2010.05424 [cond-mat.mes-hall].
[61] H. Fu, C.-X. Liu, and B. Yan, Science advances **6**, eaaz0948 (2020).
[62] D. Xiao, M.-C. Chang, and Q. Niu, Rev. Mod. Phys. **82**, 1959 (2010).
[63] D.-H. Lee and C. L. Kane, Phys. Rev. Lett. **64**, 1313 (1990).
[64] S. L. Sondhi, A. Karlhede, S. A. Kivelson, and E. H. Rezayi, Phys. Rev. B **47**, 16419 (1993).
[65] K. Moon, H. Mori, K. Yang, S. M. Girvin, A. H. MacDonald, L. Zheng, D. Yoshioka, and S.-C. Zhang, Phys. Rev. B **51**, 5138 (1995).
[66] H. A. Fertig, L. Brey, R. Côté, and A. H. MacDonald, Phys. Rev. B **50**, 11018 (1994).
[67] J.-Y. You, X.-J. Dong, B. Gu, and G. Su, Phys. Rev. B **103**, 104403 (2021).
[68] S. Du, P. Tang, J. Li, Z. Lin, Y. Xu, W. Duan, and A. Rubio, Phys. Rev. Research **2**, 022025 (2020).